*Anal. Chem.* **2002,** *74,* 1986−1992

# Steady-State Limiting Currents at Finite Conical Microelectrodes

Cynthia G. Zoski*,† and Michael V. Mirkin*,‡

*Department of Chemistry, Georgia State University, University Plaza, Atlanta, Georgia 30303, and Department of Chemistry and Biochemistry, Queens College−CUNY, Flushing, New York 11367*

**The investigation of steady-state diffusion-limiting currents at finite conical microelectrodes is reported. Such electrodes are of particular interest as probes in studies of kinetic reactions, measurements in microenvironments, and high-resolution electrochemical imaging. The diffusion-limiting currents were calculated using numerical (finite element) analysis and compared to those obtained at inlaid disk and hemispheroidal microelectrodes. Time-dependent simulations demonstrating the approach of the diffusion current to a steady-state value are also reported. The steady-state diffusion-limiting currents obtained were found to be a strong function of the electrode geometry, including the aspect ratio of the cone and the thickness of the insulating sheath. Thus, simple, approximate analytical expressions which account for these geometrical dependencies in the simulated steady-state diffusion-limited currents are also reported. As a limiting case, an analytical approximation was obtained for the steady-state current to a microdisk as a function of the insulator thickness. The use of these approximate equations in calculating electrode radii from steady-state diffusion-limiting currents is demonstrated, and good agreement was found with previously reported experimental studies. Use of the frequently implemented hemispherical theory to analyze steady-state diffusion-limiting currents obtained with finite conical microelectrodes is shown to result in an experimentally acceptable underestimation of the electrode radius.**

Since the early 1980s, the use of metal ultramicroelectrodes (UMEs) has led to significant advances in studies of heterogeneous and homogeneous reactions,[1−4] measurements in microenvironments,[5,6] and high-resolution electrochemical imaging.[7,8] Although planar disk-shaped microelectrodes[1,9−12] were initially most popular due to fabrication ease, microelectrodes of other geometries, for example, hemispheres,[1,12,13] spheres,[14,15] or rings,[12,16−18] have been used frequently in more recent studies. From a fabrication standpoint, these geometries most often involve encapsulating a metal into or onto an insulating glass sheath. [1,19−22]

Electrodes of micrometer and submicrometer dimensions have also been fabricated by electrochemical etching of carbon fibers or metal microwires to a sharp point and then coating with an insulating material except at the apex of the tip, thus providing a tiny exposed electrode area.[23−31] Insulating materials have included glass,[23,24] Apiezon wax,[32] and electrophoretic paint.[28,29,33−36] Char-

* Corresponding authors. E-mail: checgz@panther.gsu.edu. Michael_Mirkin@qc.edu.

† Georgia State University.

‡ Queens College−CUNY.

(1) Wightman, R. M.; Wipf, D. O. In *Electroanalytical Chemistry*; Bard, A. J., Ed.; Marcel Dekker: New York, 1989; Vol. 15, p 267.
(2) Montenegro, M. I. In *Research in Chemical Kinetics*; Compton, R. G., Hancock, G., Eds.; Elsevier: Amsterdam, 1999; p 1.
(3) Amatore, C. In *Physical Electrochemistry*; Rubinstein, I., Ed.; Marcel Dekker: New York, 1995; p 131.
(4) *Microelectrodes: Theory and Applications*; Montenegro, M. I., Queiros, M. A., Daschbach, J. L., Eds.; Kluwer Academic Publishers: Dordrecht, 1991.
(5) Kawagoe, K. T.; Zimmerman, J. B.; Wightman, R. M. *J. Neurosci. Methods* **1993**, *48*, 225.
(6) Clark, R. A.; Zerby, S. E.; Ewing, A. G. In *Electroanalytical Chemistry*; Bard, A. J., Rubinstein, I., Eds.; Marcel Dekker: New York, 1998; Vol. 20, p 227.
(7) Bard, A. J.; Fan, F.-R. F.; Mirkin, M. V. In *Electroanalytical Chemistry*; Bard, A. J., Rubinstein, I., Eds.; Marcel Dekker: New York, 1994; Vol. 18, p 244.
(8) *Scanning Electrochemical Microscopy*; Bard, A. J., Mirkin, M. V., Eds.; Marcel Dekker: New York, 2001.
(9) Saito, Y. *Rev. Polarogr.* **1968**, *15*, 177.
(10) Oldham, K. B. *J. Electroanal. Chem.* **1981**, *122*, 1.
(11) Shoup, D.; Szabo, A. *J. Electroanal. Chem.* **1982**, *140*, 237.
(12) Zoski, C. G. In *Modern Techniques in Electroanalysis*; Vanysek, P., Ed.; John Wiley & Sons: New York, 1996; Vol. 139, p 241.
(13) Bard, A. J.; Faulkner, L. R. *Electrochemical Methods: Fundamentals and Applications*; John Wiley & Sons: New York, 2001.
(14) Demaille, C.; Brust, M.; Tsionsky, M.; Bard, A. J. *Anal. Chem.* **1997**, *69*, 2323.
(15) Miles, D. T.; Knedlik, A.; Wipf, D. O. *Anal. Chem.* **1997**, *69*, 1240.
(16) Szabo, A. *J. Phys. Chem.* **1987**, *91*, 3108.
(17) Saraceno, R. A.; Ewing, A. G. *J. Electroanal. Chem.* **1988**, *257*, 83.
(18) Lee, Y.; Amemiya, S.; Bard, A. J. *Anal. Chem.* **2001**, *73*, 2261.
(19) Fan, F.-R. F.; Demaille, C. In *Scanning Electrochemical Microscopy*; Bard, A. J., Mirkin, M. V., Eds.; Marcel Dekker: New York, 2001, p 75.
(20) Michael, A. C.; Wightman, R. M. In *Laboratory Techniques in Electroanalytical Chemistry*; Kissinger, P. T., Heineman, W. R., Eds.; Marcel Dekker: New York, 1996; p 367.
(21) Stulik, K.; Amatore, C.; Holub, K.; Marecek, V.; Kutner, W. *Pure Appl. Chem.* **2000**, *72*, 1483.
(22) *Ultramicroelectrodes;* Fleischmann, M., Pons, S., Rolison, D. R., Schmidt, P. P., Eds.; Datatech Systems, Inc.: Morganton, NC, 1987.
(23) Penner, R. M.; Heben, M. J.; Lewis, N. S. *Anal. Chem.* **1989**, *61*, 1630.
(24) Penner, R. M.; Heben, M. J.; Longin, T. L.; Lewis, N. S. *Science* **1990**, *250*, 1118.
(25) Kawagoe, K. T.; Jankowski, J. A.; Wightman, R. M. *Anal. Chem.* **1991**, *63*, 1589.
(26) Mirkin, M. V.; Fan, R.-R. F.; Bard, A. J. *Science* **1992**, *257*, 364.
(27) Shao, Y.; Mirkin, M. V.; Fish, G.; Kokotov, S.; Palanker, D.; Lewis, A. *Anal. Chem.* **1997**, *69*, 1627.
(28) Slevin, C. J.; Gray, N. J., Macpherson, J. V.; Webb, M. A.; Unwin, P. R. *Electrochem. Commun.* **1999**, *1*, 282.
(29) Conyers, J. L., Jr.; White, H. S. *Anal. Chem.* **2000**, *72*, 4441.
(30) Maus, R.; Wightman, R. M. *Anal. Chem.* **2001**, *73*, 3993.
(31) Macpherson, J. V.; Unwin, P. R. *Anal. Chem.* **2000**, *72*, 276.
(32) Nagahara, L. A.; Thundat, T.; Lindsay, S. M. *Rev. Sci. Instrum.* **1989**, *60*, 3128.



10.1021/ac015669i CCC: $22.00 
Published on Web 04/05/2002

acterization of the insulated etched electrodes is carried out by combination of scanning electron microscopy (SEM), steady-state voltammetry (SSV), and, more recently, scanning electrochemical microscopy (SECM). From SEM micrographs, the shape of etched electrodes has most often been described as conical because they are sharp at the apex and broad at the base where the metal and insulator meet.[23−27] Steady-state voltammetric experiments produce retraceable, sigmoidal current versus potential (*i*−*E*) curves, which are characteristic of ultramicroelectrodes.[23−30] SECM experiments using etched electrodes as the tip electrode have shown that the geometry is closer to conical than to either a disk or a hemisphere.[26,37]

The use of finite conical electrodes for quantitative experiments has been severely limited by the absence of theory to describe their behavior under even the simplest electrochemical conditions. Earlier, Aoki[38] solved the time-dependent problem for a diffusion-controlled process at an infinite conical electrode when the potential has been stepped to the limiting current region and also derived a long-time approximation for a sharply spired electrode, which is not relevant to the present study. Sokirko and Oldham[39] later confirmed the work of Aoki in a similar study of an infinite conical electrode. Several theoretical analyses also exist for a finite conical electrode in an SECM configuration, as the finite cone approaches either a conducting or an insulating surface.[37,40,41] However, these investigations do not address the diffusion-limited current specifically.

We report here the study of the steady-state current at a finite conical electrode under diffusion-limiting conditions and compare the response to that of a disk electrode and the closely related hemispheroidal electrode.[42−45] The numerical solution of the partial differential equations was carried out with PDEase 2D,[46,47] a commercial program employing finite element analysis. The simulated data were fitted to approximate analytical expressions to describe the dependence of the limiting current on the aspect ratio of a finite conical electrode and the thickness of the insulating sheath. Although it is intuitive that the current to a small UME under potentiostatic conditions should quickly reach a steady state, no theoretical proof of the steady-state response of finite conical electrodes has yet been presented. Thus, we report time-dependent simulations demonstrating that the diffusion current at a finite cone decays to a steady-state value.


(33) Schulte, A.; Chow, R. H. *Anal. Chem.* **1996**, *68*, 3054.
(34) Bach, C. E.; Nichols, R. J.; Meyer, H.; Besenhard, J. O. *Surf. Coatings Technol.* **1994**, *67*, 139.
(35) Bach, C. E.; Nichols, R. J.; Beckman, W.; Meyer, H.; Shulte, A.; Besenhard, J. O. Jannakoudakis, P. D. *J. Electrochem. Soc.* **1993**, *140*, 1281.
(36) Mao, B. W.; Ye, J. H., Zhuo, X. D.; Mu, J. Q.; Fen, Z. D.; Tian, Z. W. *Ultramicroscopy* **1992**, *42*−*44*, 464.
(37) Mirkin, M. V.; Fan, F.-R. F.; Bard, A. J. *Electroanal. Chem.* **1992**, *328*, 47.
(38) Aoki, K. *J. Electroanal. Chem.* **1990**, *281*, 29.
(39) Sokirko, A. V.; Oldham, K. B. *J. Electroanal. Chem.* **1997**, *430*, 15.
(40) Davis, J. M.; Fan, F.-R. F.; Bard, A. J. *J. Electroanal. Chem.* **1987**, *238*, 9.
(41) Fulian, Q.; Fisher, A. C.; Denuault, G. *J. Phys. Chem. B* **1999**, *103*, 4387.
(42) Birke, R. L. *J. Electroanal. Chem.* **1989**, *274*, 297.
(43) Oldham, K. B. *J. Electroanal. Chem.* **1990**, *284*, 491.
(44) Myland, J. C.; Oldham, K. B. *J. Electroanal. Chem.* **1990**, *288*, 1.
(45) Birke, R. L.; Huang, Z. *Anal. Chem.* **1992**, *64*, 1513.
(46) PDEase2D, Version 3.0, Macsyma, Inc., Arlington, MA, 1982−1998.
(47) Mirkin, M. V. In *Scanning Electrochemical Microscopy*; Bard, A. J., Mirkin, M. V., Eds.; Marcel Dekker: New York, 2001; Chapter 4.


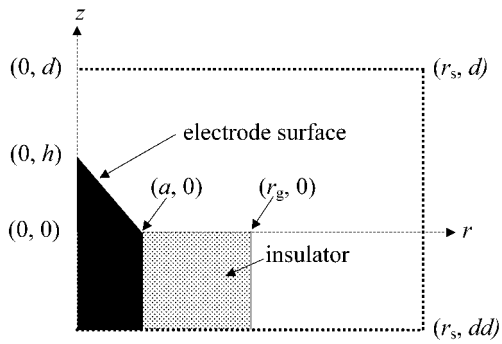


Figure 1. Diagram of a finite conical electrode in cylindrical coordinates and geometry of the simulation space.

## THEORY OF FINITE CONICAL ELECTRODES

The geometry of a finite conical electrode is described by three parameters: the base radius ($a$) of the cone, the height ($h$), and the radius of the insulating sheath ($r_g$), as shown in Figure 1, or, alternatively, by $a$, $r_g$, and the aspect ratio $H = h/a$.

Consider a one-step reaction

$$\mathrm{O\ (soln)} + n\mathrm{e} \rightarrow \mathrm{R\ (soln)} \tag{1}$$

taking place at a finite conical electrode surface surrounded by insulation (Figure 1) under conditions in which species O reaches and species R leaves the electrode solely by diffusion. The diffusion equation in cylindrical coordinates is

$$\frac{\partial c}{\partial t} = D\left(\frac{\partial^2 c}{\partial r^2} + \frac{1}{r}\frac{\partial c}{\partial r} + \frac{\partial^2 c}{\partial z^2}\right) \tag{2}$$

where $r$ and $z$ are the coordinates in directions parallel and normal to the electrode base plane, respectively, $t$ represents time, $c(r,z,t)$ is the concentration, and $D$ is the diffusion coefficient of species O. For convenience, normalized dimensionless variables are introduced as follows,

$$T = Dt/a^2 \tag{3a}$$

$$R = r/a \tag{3b}$$

$$Z = z/a \tag{3c}$$

$$C = c(r,z,t)/c \tag{3d}$$

$$H = h/a \tag{3e}$$

$$L = d/a \tag{3f}$$

$$LL = dd/a \tag{3g}$$

$$RG = r_g/a \tag{3h}$$

$$RS = r_s/a \tag{3i}$$

where $a$ is the base radius of the cone, $c$ is the bulk concentration of O, $r_g$ is the insulator radius, $d$ and $r_s$ are the simulation space limits in normal and radial directions, and $dd$ is the distance to the simulation limit behind the electrode surface.

To calculate the diffusion-limiting current to the conical surface, eq 4 in dimensionless form

$$\frac{\partial C}{\partial T} = \frac{\partial^2 C}{\partial R^2} + \frac{1}{R}\frac{\partial C}{\partial R} + \frac{\partial^2 C}{\partial Z^2} \qquad 0 \le R \le RS,\ LL < Z < L \quad (4)$$

was solved with the following initial and boundary conditions:

initial condition

$$C(R,Z,0) = 1 \qquad 0 \le R \le 1,\ H(1-R) < Z < \mathrm{L} \quad \text{and}$$
$$1 \le R < RG,\ 0 < Z < L \quad \text{and}$$
$$RG < R < RS,\ LL < Z < L \quad (5)$$

cone surface

$$C(R,H(1-R),T) = 0 \qquad 0 \le R \le 1 \quad (6)$$

insulation region

$$(\partial C(R,Z,T)/\partial Z)_{Z=0} = 0 \qquad 1 \le R \le RG \quad (7)$$

simulation space limit

$$C(R,Z,T) = 1 \qquad 0 \le R \le RS,\ Z = L \quad \text{and}$$
$$R = RS,\ LL \le Z \le L \quad \text{and} \quad RG \le R \le RS,\ L = LL \quad (8)$$

axis of symmetry

$$(\partial C(R,Z,T)/\partial R)_{R=0} = 0 \qquad H \le Z \le L \quad (9)$$

insulation below base plane

$$(\partial C(R,Z,T)/\partial R)_{R=RG} = 0 \qquad LL \le Z < 0 \quad (10)$$

The time-dependent eq 4 was solved numerically to investigate the transient approach of the current at a finite cone to its limiting steady-state value. The results of the time-dependent simulations were compared to those obtained from the steady-state diffusion equation

$$\frac{\partial^2 C}{\partial R^2} + \frac{1}{R}\frac{\partial C}{\partial R} + \frac{\partial^2 C}{\partial Z^2} = 0 \quad (11)$$

Steady-state simulations based on eq 11 were performed with the same boundary conditions (eqs 6−10) by assuming that concentration is a function of $R$ and $Z$ only ($\mathrm{C} = C(R,Z)$). The current (either time-dependent or steady state) to the finite conical electrode was obtained by integrating the flux over the cone side ($L_c$)

$$i_{\mathrm{cone}} = 2\pi nFDca\int_0^{L_c} R(\partial C/\partial N)\,\mathrm{d}X \quad (12)$$

where $\partial C/\partial N = (\partial C/\partial Z \cos\alpha + \partial C/\partial R \sin\alpha)_{Z=H(1-R)}$ is the normal derivative of concentration at the finite cone surface, $\alpha$ is the angle at the base of the cone, $L_c = 1/\cos\alpha$, and $X$ is the integration variable.

Finally, the current to the finite conical electrode surface can be normalized by the steady-state limiting current at a disk of the same radius, which represents the $H = 0$ limit of the conical geometry

$$I_{\mathrm{cone}} = i_{\mathrm{cone}}/i_{\mathrm{disk}}^{\mathrm{ss}} = 0.5\pi\int_0^{L_c} R(\partial C/\partial N)\,\mathrm{d}X \quad (13)$$

where

$$i_{\mathrm{disk}}^{\mathrm{ss}} = 4nFDca \quad (14)$$

## STEADY-STATE AND TIME-DEPENDENT SIMULATIONS WITH PDEASE 2D

Equations 4 and 11 were solved numerically using the PDEase 2D program package on a 866-MHz Pentium III PC. This program uses a Galerkin finite element solver and creates a triangular adaptive grid, which allows problems involving singularities to be solved with high accuracy and computational efficiency. PDEase 2D was used previously to simulate the responses of microdisk and ring electrodes,[18,47,48] and several examples of the user input files required for such calculations were discussed in ref 47. To achieve the balance between accuracy and simulation efficiency, PDEase 2D sets up a coarse space grid according to the initial and boundary conditions. An iterative process is used to refine this grid until the acceptable error criteria are satisfied. At the end of each iteration, PDEase2D determines the error for each cell of the grid and subdivides those cells in which the error exceeds the user-specified ERRLIM value. Typically, the final grid has a high density of nodes near the electrode surface and much lower density at the periphery of the simulation space.

In all simulations, our goal was to keep the relative error below 1% of the absolute value of the calculated current. This was achieved by setting the ERRLIM value between $10^{-5}$ and $10^{-7}$, depending on electrode geometry. Simulation results were considered acceptable when decreasing ERRLIM by the factor of 2−5 produced negligible (i.e., ≪1%) change in the calculated current. Another sign of accuracy of the obtained numerical solution was the absence of oscillations and discontinuities in the simulated concentration profiles and flux distribution over the electrode surface.

The ERRLIM statement also determines the number of cells and nodes that are created. When the error obtained using the initial coarse grid is much larger than the specified error limit, PDEase2D increases the density of nodes in the grid very quickly. This may greatly decrease the computation efficiency and result in an unreasonably long running time. The sharper the cone, the harder it is for the solver to achieve convergence at a specified error limit, and the more cells and nodes it creates. The creation of extra nodes by PDEase2D was suppressed by assigning a low value to the BALANCE parameter (e.g., 0.2 for steady-state simulation of a fairly sharp cone, or even 0.0075 for a transient at a very sharp cone, $H = 10$). The proper choice of two other parameters (CONVERGE and SUBCONVERGE) can also improve the efficiency of simulation by ensuring that the solver does not terminate the iteration prematurely, thus avoiding unnecessary regridding. A typical two-dimensional final grid generated by PDEase2D for a steady-state simulation comprised between 2500 and 20 000 cells (5000−40 000 nodes).

To check that the simulation domain is sufficiently large to be considered essentially infinite, we investigated the effect of

(48) Shao, Y.; Mirkin, M. V. *J. Phys. Chem. B* **1998**, *102*, 9915.

increasing (or decreasing) the *L*, *LL*, and *RS* values, which set the simulation space limits. It was found that simulation results changed very little when the *L*, *LL*, and *RS* values were increased from 50 to 100. Any further expansion of the simulation space resulted in a significantly less than 1% change in diffusion currents. Thus, $L = RS = 100$ and $LL = -50$ were used in both steady-state and time-dependent simulations.

Running times of 5−25 min were common for steady-state simulations. For time-dependent simulations, PDEase2D uses a self-adjusting evolution solver. This solver reduces the time step when it encounters a region of rapid change and increases the interval when the concentration profile becomes more steady. The size of the time step is also influenced by the value of ERRLIM. When the requested error limit is not readily achieved, the time step may become extremely small, so that the running time increases greatly. Extensive experimentation with ERRLIM and BALANCE parameters is required to eliminate this problem. The current transients at a blunt cone (i.e., $H \ll 1$) are similar to those obtained at microdisk electrodes. Hence the times required to approach steady state to within 1−2% are of the order of $100a^2/D$. In contrast, it takes a significantly (by the factor of ∼10) longer time for a diffusion current at a sharper cone (e.g., $H > 3$) to approach the steady state. Most simulations of transients required no more than 45 min of running time.

## RESULTS AND DISCUSSION

**Transient Currents.** To confirm the accuracy of the simulation model for the finite cone, transient currents at an inlaid disk electrode with infinite *RG* (*RG* = 100) were first simulated. The transient and steady-state behavior of inlaid disk electrodes is well documented.[9−11,49−50] Shoup and Szabo provided a single empirical relationship for a diffusion-controlled process covering the entire time range, from transient to steady state, with an accuracy better than 0.6% at all points[11]

$$I_{\text{disk}}(\tau) = \frac{i_{\text{disk}}(\tau)}{i_{\text{disk}}^{\text{ss}}} = 0.7854 + 0.8862\tau^{-1/2} + 0.2146\exp(-0.7823\tau^{-1/2}) \quad (15)$$

where $\tau = 4Dt/a^2$. Table 1 shows that the results of our simulations agree well (within 0.1−0.7%) with the currents calculated from the Shoup and Szabo equation.

Simulated current transients for the finite conical electrode geometry were obtained for aspect ratios $H = 0.5$, 1, 2, 3, and 10. The results for $H = 0.5$, 1, 2, and 3, are shown in Figure 2. The solid line at $H = 0$ corresponds to the transient current for an inlaid disk electrode, calculated from eq 15, which initially is Cottrellian in behavior and then approaches a normalized steady-state value equal to unity, as expected. The conical electrodes exhibit similar behavior, as Figure 2a demonstrates. However, as the aspect ratio *H* increases, the time required to approach within 1% of the steady state also increases from $\tau/4 = 600$ for $H = 0.5$ to $\tau/4 = 1000$ for $H = 3$, as shown in Figure 2b. Additionally, the steady-state current value, relative to the inlaid disk of equal radius, increases above unity. The dashed lines in Figure 2b represent steady-state current values obtained for each *H* by solving steady-state diffusion eq 11. Table 2 shows the comparison of the steady-state current values obtained from the transient simulations with those from the steady-state simulations. All long-time transient current values were within 0.2% of the steady-state values.

**Diffusion-Limited Steady-State Currents.** The steady-state currents at finite cones ranging from $H = 0$ to $H = 5$ were

Table 1. Normalized Currents at an Inlaid Disk Microelectrode[a]

| $\tau$ | eq 15[51] | simulation[b] |
|---|---|---|
| 0.04 | 5.221 | 5.232 |
| 0.4 | 2.249 | 2.245 |
| 4 | 1.374 | 1.365 |
| 40 | 1.115 | 1.113 |
| 400 | 1.036 | 1.035 |
| 800 | 1.025 | 1.024 |
| 1200 | 1.021 | 1.020 |
| 1600 | 1.018 | 1.017 |
| 2000 | 1.016 | 1.015 |
| 2400 | 1.015 | 1.014 |
| 2800 | 1.014 | 1.013 |
| 3200 | 1.013 | 1.012 |
| 3600 | 1.012 | 1.011 |
| 4000 | 1.011 | 1.010 |
| 8000 | 1.008 | 1.007 |
| 12000 | 1.007 | 1.006 |

[a] $I_{\text{disk}}(\tau) = i_{\text{disk}}(\tau)/i_{\text{disk}}^{\text{ss}} = i_{\text{disk}}(\tau)/4nFDca$. [b] Calculated for $RG = 100$.

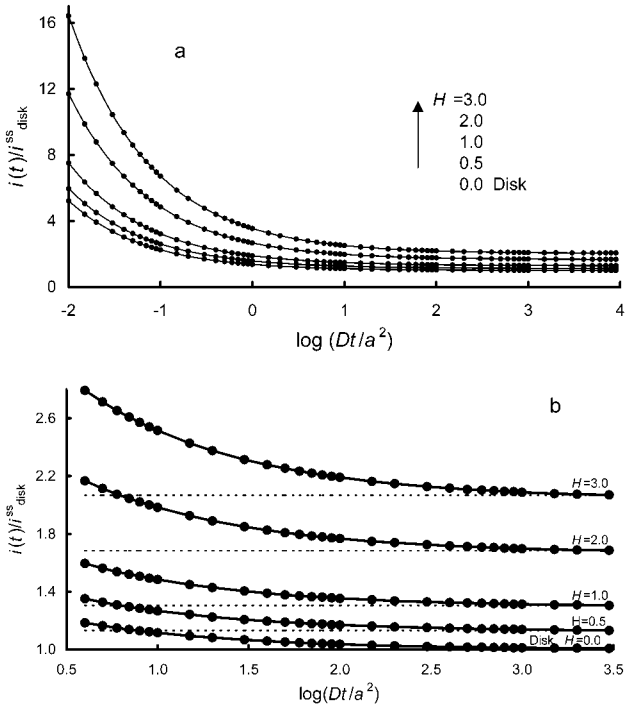


Figure 2. Simulated current transients for different aspect ratios (*H*). The currents are normalized by the steady-state current at the microdisk electrode of the same radius (eq 14). In (a) and (b), the solid line at $H = 0$ is based on eq 15. The solid lines for other reported *H* values represent the best fit through the series of points. In (b), the dashed lines correspond to the steady-state limiting current values for each finite conical electrode.


(49) Bond, A. M.; Oldham, K. B.; Zoski, C. G. *J. Electroanal. Chem.* **1988**, *245*, 71.

(50) Oldham, K. B.; Zoski, C. G. *J. Electroanal. Chem.* **1988**, *256*, 11.

Table 2. Comparison of Simulated Long-Time Transient Currents ($T = 9000$) and Steady-State Limiting Currents at a Microcone[a]

| | $i_{cone}(T)/i^{ss}_{disk}$ | $i^{ss}_{cone}/i^{ss}_{disk}$ | |
|---|---|---|---|
| $H$ | simulation | simulation | eq 16 |
| 0[b] | 1.006 | 1.004 | 1.000 |
| 0.5 | 1.131 | 1.131 | 1.139 |
| 1 | 1.303 | 1.304 | 1.307 |
| 2 | 1.683 | 1.684 | 1.678 |
| 3 | 2.066 | 2.068 | 2.078 |
| 5 | 2.802 | 2.805 | |
| 10 | 4.501 | 4.511 | |

[a] $RG = 100$; $i^{ss}_{disk} = 4nFDca$. [b] At $H = 0$, the shape of the electrode is a disk.

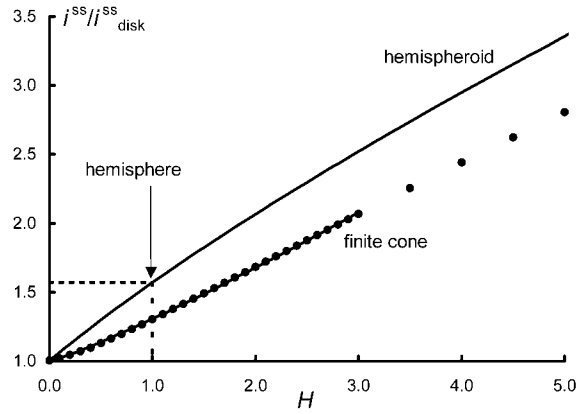


Figure 3. Comparison of steady-state currents for a hemispheroid (eq 18) and a finite cone: (●) simulated points; (—) eq 16.

simulated and are graphed in Figure 3. Several of these values are compared with those from the long-time transients in Table 2, where the agreement is found to be excellent. An analytical approximation, which fits simulated normalized currents to finite conical electrodes for $H$ values between 0 and 3 to within 1% (Figure 3), is found to be of the form

$$I^{ss}_{cone} = i^{ss}_{cone}/i^{ss}_{disk} = 1 + qH^p \qquad (16)$$

where $H = h/a$, $q = 0.30661$, and $p = 1.144\,66$. Equation 16 was restricted to aspect ratios between 0 and 3, since this is the range in which values have been reported experimentally.[23,26,37] The solid line in Figure 3 represents eq 16, from which the steady-state diffusion-limiting current to a finite cone can be expressed as

$$i^{ss}_{cone} = 4nFDca(1 + qH^p) \qquad (17)$$

Of the many shapes of microelectrodes that have been reported, finite cones most closely resemble hemispheroidal microelectrodes,[43,44] which are also parametrized by an aspect ratio $H$. It is thus of interest to compare the steady-state limiting currents of the two electrode geometries. A hemispheroidal microelectrode has also been referred to as a "conforming microelectrode" because it rests on an infinite insulating plane, it is symmetrical with respect to rotation around an axis perpendicular to the insulating plane, the line of intersection of the electrode with the insulating plane is a single circle, and the electrode achieves a maximum distance $h$ above the insulating plane of the electrode.[44] Other well-known conforming microelectrodes include the hemisphere and inlaid disk microelectrodes. A common feature of all conforming microelectrodes is that they achieve true voltammetric steady states. These criteria also apply to the finite cone, and thus support our simulation results which demonstrate that a steady state is reached after an initial transient period.

Hemispheroidal microelectrodes whose height is smaller than the radius ($h < a$ or $H < 1$) are referred to as "oblate hemispheroids", while those with a height greater than the radius ($h > a$ or $H > 1$) are referred to as "prolate hemispheroids".[44] The steady-state limiting current for each is

$$i^{ss}_{hemispheroid} = \begin{cases} 2\pi nFDca\sqrt{1 - H^2}/\arccos(H) & \text{when } H < 1 \\ 2\pi nFDca\sqrt{H^2 - 1}/\operatorname{arccosh}(H) & \text{when } H > 1 \end{cases} \qquad (18)$$

The hemispheroidal steady-state limiting currents as a function of $H$ are graphed in Figure 3 for comparison with the results for a finite cone. The hemispherical limit is indicated by the dashed line at $H = 1$. The increase in the steady-state current with $H$ is qualitatively similar for hemispheroidal microelectrodes and finite cones. The area of a hemispheroid is larger than that of a finite cone with the same radius value $a$ and aspect ratio $H$, and this results in the larger current observed for the hemispheroid in Figure 3. For example, at $H = 1$, the hemispheroid is a hemisphere of area $2\pi a^2$. The corresponding finite cone at $H = 1$, has an area (see eq 21) of $2^{1/2}\pi a^2$.

**Effect of Insulating Sheath Thickness on the Steady-State Diffusion-Limiting Current.** Shoup and Szabo[51] were the first to demonstrate that diffusion from behind the plane of an electrode enhances the flux to an inlaid disk significantly when the insulating sheath thickness is comparable to the disk radius (i.e., $RG = r_g/a$ is close to 1). They used a hopscotch algorithm to solve eq 2. Fang and Leddy[52] used a standard explicit finite difference (EFD) method with a fixed time grid and exponentially expanding spatial grid (EESG) to confirm and expand on the work of Shoup and Szabo. From their simulation data, they proposed an approximate analytical expression for the steady-state current as a function of $RG$. Amphlett and Denault[53] returned to this problem because of the importance of the $RG$ value for SECM theory. Their simulations employed the finite difference alternating-direction implicit (ADI) method. Because we reference our conical steady-state currents with respect to those at the corresponding inlaid disk, we were interested in comparing the values of our simulations, based on eqs 6−11 with $H = 0$, to the previously reported data. As can be seen in Figure 4, the results of our simulations agree more closely with those from refs 51 and 53, while the current values from ref 52 are somewhat higher.

(51) Shoup, D.; Szabo, A. *J. Electroanal. Chem.* **1984**, *160*, 27.
(52) Fang, Y.; Leddy, J. *Anal. Chem.* **1995**, *67*, 1259.
(53) Amphlett, J. L.; Denault, G. *J. Phys. Chem. B* **1998**, *102*, 9946.

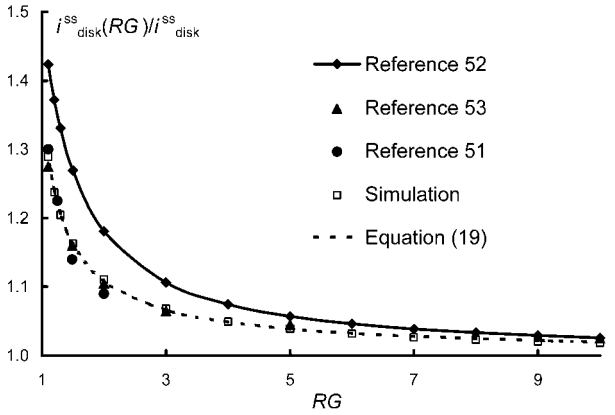


Figure 4. Effect of the sheath thickness (*RG*) on the steady-state limiting current at a disk electrode.

Table 3. Normalized Diffusion Current to a Conical Electrode ($I^{ss}_{cone} = i^{ss}_{cone}(RG/4nFDca)$ as a Function of *H* and *RG*

| | $I^{ss}_{cone}$ | | | | |
|---|---|---|---|---|---|
| RG | $H = 0.0$ | $H = 0.5$ | $H = 1.0$ | $H = 2.0$ | $H = 3.0$ |
| 100 | 1.000 | 1.131 | 1.302 | 1.684 | 2.067 |
| 10 | 1.018 | 1.152 | 1.330 | 1.731 | 2.139 |
| 9 | 1.020 | 1.155 | 1.334 | 1.737 | 2.148 |
| 8 | 1.023 | 1.159 | 1.339 | 1.745 | 2.160 |
| 7 | 1.027 | 1.164 | 1.345 | 1.756 | 2.175 |
| 6 | 1.032 | 1.170 | 1.354 | 1.769 | 2.195 |
| 5 | 1.039 | 1.178 | 1.365 | 1.788 | 2.223 |
| 4 | 1.050 | 1.192 | 1.383 | 1.818 | 2.264 |
| 3 | 1.068 | 1.217 | 1.414 | 1.867 | 2.330 |
| 2 | 1.110 | 1.270 | 1.483 | 1.968 | 2.456 |
| 1.5 | 1.163 | 1.336 | 1.564 | 2.073 | 2.575 |
| 1.2 | 1.238 | 1.425 | 1.665 | 2.192 | 2.695 |

The current versus *RG* dependence for a microdisk electrode can be described by an approximate analytical expression

$$i^{ss}_{disk}(RG)/i^{ss}_{disk} = 1.0000 + B(RG - C)^D \qquad (19)$$

where $B = 0.1380$, $C = 0.6723$, and $D = -0.8686$. The normalized current values obtained from this equation, which fits to within 0.2% the results of our steady-state simulations for $1.1 \le RG \le 100$, are shown by the dashed line in Figure 4. The steady-state current to a microdisk electrode is enhanced by 2% at $RG = 10$, by 4% at $RG = 5$, and by 30% at $RG = 1.1$ over the current to a disk embedded into an infinitely thick insulator.

Similar to disk electrodes, the diffusion-limiting current at a finite cone also increases with decreasing *RG*. Table 3 presents the values of $I^{ss}_{cone}$ as a function of *H* and *RG* relative to an inlaid disk of identical radius and with infinite *RG*. These simulated, normalized current values of Table 3 are approximated to within an accuracy of ±0.2% by the approximate analytical expression

$$I^{ss}_{cone} = i^{ss}_{cone}/i^{ss}_{disk} = A + B(RG - C)^D \qquad (20)$$

as demonstrated in Figure 5. The constants *A*, *B*, *C*, and *D* are tabulated for different *H* values in Table 4. One should notice that, at $H = 0$, eq 20 becomes identical to eq 19 for a disk.

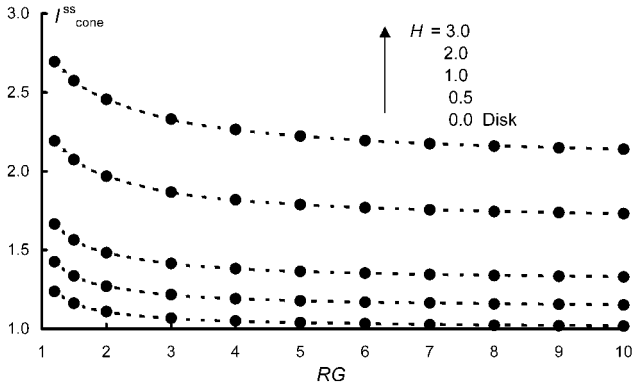


Figure 5. Comparison of simulation data of Table 3 and $I^{SS}_{cone}$ calculated from equation 20: (●) simulated points; (—) eq 20.

Table 4. Numerical Constants Corresponding to the Approximate Analytical Eq 20

| | $H = 0$ | $H = 0.5$ | $H = 1$ | $H = 2$ | $H = 3$ |
|---|---|---|---|---|---|
| *A* | 1.0000 | 1.1270 | 1.2979 | 1.6769 | 2.0585 |
| *B* | 0.1380 | 0.1972 | 0.2795 | 0.5240 | 0.8910 |
| *C* | 0.6723 | 0.5667 | 0.4506 | 0.1794 | −0.1900 |
| *D* | −0.8686 | −0.9025 | −0.9436 | −0.9857 | −1.0288 |

**Comparison with Previous Experimental Studies.** Penner et al.[23] were the first to try to quantitatively characterize microelectrodes which they fabricated by etching Pt−Ir wire followed by coating with poly(α-methylstyrene) as a means of insulating the electrode body but not the electrode tip. These electrodes were characterized by SEM, cyclic voltammetry, and chronoamperometry in a solution of 4.21 mM $Fe(CN)_6^{4-}$/0.5 M $Na_2SO_4$ in which the diffusion coefficient of ferrocyanide is $D = 7.94 \times 10^{-6}$ cm$^2$. From the SEM images, they measured an aspect ratio, $H = h/a = 2.4$ (The parameter used in ref 23 was $\alpha = h/2a = 1.2$; this corresponds to $H/2$ in our notation). Retraceable sigmoidal-shaped current−potential curves were obtained using cyclic voltammetry, indicative that a steady state had been reached. Chronoamperometric plots of *i* versus $t^{-1/2}$ were found to be linear for times between 70 μs and 0.01 s. The slopes of the chronoamperometric plots were then used to calculate a value for the surface area of the etched electrodes from the Cottrell equation. For a conical electrode, the lateral surface area is given by eq 21

$$A_{cone} = \pi a^2(H^2 + 1)^{1/2} \qquad (21)$$

from which the electrode radius *a* is found. The electrode radii calculated in ref 23 using the Cottrell equation are compared in Table 5 to those obtained from the steady-state analytical approximation (eq 17). The agreement between the two sets of calculated values is reasonable considering that there is no information on the thickness of the insulating polymer layer.

Recently, SECM was used to evaluate the tip shapes of nanometer-sized microelectrodes.[26,37] In this method, the tip electrode was brought in close proximity to a conducting or insulating surface and the resulting experimental tip current versus distance curve was compared to a family of theoretical working curves computed for different values of the height (or

Table 5. Comparison of Electrode Radii Determined in Ref 23 with Those Calculated from Eq 17

| $A_{cone}$, cm$^2$ | $H$ | $a$, $\mu$m (eq 21) | $I^{ss}_{cone}$, nA | $a$, $\mu$m (eq 17) |
|---|---|---|---|---|
| $3.46 \times 10^{-6}$ | 2.4 | 6.53 | 13.2 | 5.56 |
| $1.91 \times 10^{-6}$ | 2.4 | 4.84 | 9.73 | 4.11 |
| $1.81 \times 10^{-7}$ | 2.4 | 1.49 | 3.44 | 1.45 |

aspect ratio) of a conical electrode. A 0.178 M $K_4Fe(CN)_6$/2 M HCl solution with a reported diffusion coefficient $D = 6.22 \times 10^{-6}$ cm$^2$/s, was used. The Pt−Ir tip electrode was prepared by electrochemical etching and insulated with molten Apiezon wax. The diffusion-limiting current, $i^{ss}_{cone} = 1.8$ nA was recorded at distances far from a conducting substrate. From the SECM fitting procedure, the radius $a = 30$ nm and aspect ratio $H = 1$ were found. Substituting these experimental values into the analytical approximation 17, leads to a calculation of $a = 32$ nm, which is in good agreement with the experimentally determined value of 30 nm. Using the $H = 1$ column of Table 3, it is possible to look at the effect of $RG$ on the calculated $a$ value from expression 17. For example, for $RG = 5$

$$i^{ss}_{cone}(RG = 5) = 1.365 i^{ss}_{disk} = 1.365 \times 4nFDca \quad (22)$$

so that the current to a conically shaped electrode with the aspect ratio $H = 1$ and basal radius $a$ is larger than that to a disk of the same radius by the factor of 1.365. Thus, for $i^{ss}_{cone} = 1.8$ nA, an estimated value of radius $a$ is 31 nm. For $RG = 10$, 3, 2, 1.5 and 1.2, corresponding values of $a$ are found to be 32, 30, 28, 27, and 25 nm. Thus, assuming that the error in a determination is ≤10%, the $RG$ value for this particular electrode seems to be ≥3. The same conclusion could be reached by using eq 20.

**Radius Determination Based on Hemispherical Model.** In studies with etched electrodes, it is common practice to assume that the active part of the electrode is hemispherical in shape[24,28,29,31] and calculate a radius based on the diffusion-limited steady-state current expressed as eq 23 for a microhemisphere

$$i^{ss}_{hemisphere} = 2\pi nFDcr_o \quad (23)$$

where $r_o$ is the hemisphere radius surrounded by an infinite insulating sheath. If the actual geometry of the etched electrode is conical, the combination of eq 23 with eq 17 yields

$$\pi r_o = 2a(1 + qH^p) \quad (24)$$

and assuming that a finite cone most closely approximates a hemisphere when $H = 1$, one finds

$$r_o = (2a/\pi)(1 + q) = 0.832a \quad (25)$$

where $q$ is defined in eq 16. Equation 25 indicates that the hemispherical radius is 83% of the finite conical basal radius. Thus, the use of the hemispherical theory to analyze the data obtained with a small conical electrode results in a 17% underestimation of the tip radius.

From an experimental point of view based on SEM images, the assumption of a perfect finite conical shape has been shown to be doubtful for submicrometer-sized electrodes. The uncertainties in an etched electrode will include the insulating sheath thickness, the aspect ratio and the exact shape (blunt or pointed) of the tip end of the electrode. Unless the electrode geometry is thoroughly characterized (e.g., by SECM), the use of the simpler hemispherical model for data analysis appears to be within the limits of acceptable experimental error.

## ACKNOWLEDGMENT

The support by the donors of the Petroleum Research Fund administrated by the American Chemical Society, a grant from PSC−CUNY (M.V.M.), and a GSU Research Initiation Grant (C.G.Z.) are gratefully acknowledged.

Received for review November 1, 2001. Accepted February 22, 2002.

AC015669I